A Modularized Two-Stage Active Cell Balancing Circuit for Series Connected Li-Ion Battery Packs

Kenguru Manjunath
Dept. of Electrical & Electronics Engineering
National Institute of Technology, Karnataka, Surathkal
Mangalore, India
manjunath3021@gmail.com

Kalpana R
Dept. of Electrical & Electronics Engineering
National Institute of Technology, Karnataka, Surathkal
Mangalore, India
kalpana@nitk.edu.in

2022 IEEE International Conference on Power Electronics, Drives and Energy Systems (PEDES) | 978-1-6654-5566-4/22/$31.00 ©2022 IEEE | DOI: 10.1109/PEDES56012.2022.10080471

***Abstract*— This paper addresses a modularized two-stage active cell balancing topology based on an improved buck-boost converter for a series connected Lithium-ion battery string. The proposed topology has a modular structure, each module consisting of three cells, two inductors, and four MOSFET switches. This technique provides module-to-module balancing in the first stage. Moreover, it can simultaneously target and balance two cells in a module in the second stage. Thus, significantly reduces the cell balancing time and increases the system performance with minimal components. The proposed topology has been theoretically analyzed and experimentally verified with a laboratory prototype. The proposed modularization technique is verified experimentally with two modules tested together in a battery string.**

Keywords—Active cell balancing, buck-boost converter, cell balancing speed, Li-ion battery string.

I. INTRODUCTION

Lithium-ion batteries are widely used in many applications such as electric vehicle, renewable energy and uninterruptible power supplies due to their high-power density, energy density, low self-discharge rate and high conversion efficiency. The battery pack in electric vehicle requires hundreds of volts and thousands of kilowatts output power. However, the terminal voltage of the Li-ion battery cell is small. Therefore, in medium to high power applications, a large number of cells need to be connected in series to provide the voltage requirements for the battery string. Normally, for such applications, a bi-directional power converter is used to charge and discharge the entire battery string. Ideally, the series-connected batteries with the same charge capacity should have the same terminal voltages. However, due to manufacturing tolerance, unequal ageing and temperature distribution, there is always a variation between cells' voltage in the battery string. Hence, if the Battery Management System (BMS) monitors only the terminal voltage of series connected battery string, then the battery having a lower voltage than others can be overcharged or depleted even if the string voltage is within the acceptable limits. Alternatively, if the BMS monitors each battery voltage. In that case, it has to stop charging/discharging when the terminal voltage of the battery with the lowest voltage reaches its limit, leading to increase the system performance. Therefore, a reliable voltage-balancing circuit must be provided for the series-connected batteries.

The topologies for voltage balancing circuits available in literature can be broadly classified into passive and active techniques. In passive techniques, overcharged batteries are discharged through the dissipating resistors [1]. This technique is low-cost and easy to control, but it may not be suitable in medium to high-power applications due to its high energy dissipation [2]. Hence, the passive cell balancing technique is mainly employed in low-power applications.

To overcome the limitations of passive cell balancing topologies, the active cell balancing topologies are utilized to balance the charge between the unbalanced cells. Regarding energy transfer, active cell balancing topologies can be principally categorised as adjacent cell-to-cell (AC2C), cell-to-stack (C2S), stack-to-cell (S2C) and direct cell-to-cell (DC2C).

In AC2C topologies, a bi-directional power converter is employed to transfer charge between two nearby cells. Switched capacitors [3], [4] and bi-directional buck-boost converters [5]-[7] are good choices for the AC2C methods. The main drawback of this technique is that the charge can exchange between two adjacent cells only. Hence, it requires more equalization time and low charge transfer efficiency. In C2S topologies, the charge can be transferred from one cell to the entire stack or vice-versa. Multi-winding transformers [8], multiple-transformers [9] and modularized switching transformers [10] are utilized for implementing C2S or S2C topologies. These topologies are limited in terms of transformer windings and are expensive. Moreover, some cells are unnecessarily involved in the equalization process, leading to lower balancing speed. In DC2C topologies, the charge can be transferred from a highly-charged cell to low charged cell. The equalization topology presented in [11] requires more switches or diodes to combine unbalanced cells with an inductor. Noteworthy, only one inductor participates in the equalization process; one healthy and one weak cell can simultaneously be involved in the equalization process. Thus, it requires more equalization time for a long series battery string.

To overcome the limitations in the above-mentioned literature and to aid in enhancing the balancing speed, this paper addresses a modularized two-stage active cell balancing circuit based on the improved buck-boost converter. The following are salient features of the proposed circuit over the conventional methods,

1) By transferring the high balancing current from the high to the weakest cell in a module directly, the proposed cell balancing circuit significantly reduces the balancing time with fewer components.
2) Equalization is not only confined among the cells, but it is also feasible between two unbalanced modules simultaneously.
3) Due to modulization technique used in the proposed balancing circuit reduces the voltage stress on the switches in a long string, which can greatly improve the system performance.

The rest of the paper is organized as follows. The circuit structure, operational principle, equalizing current formulation and control strategy are described in Section II. Section III describes the simulation and experimental results and Section IV concludes this paper.

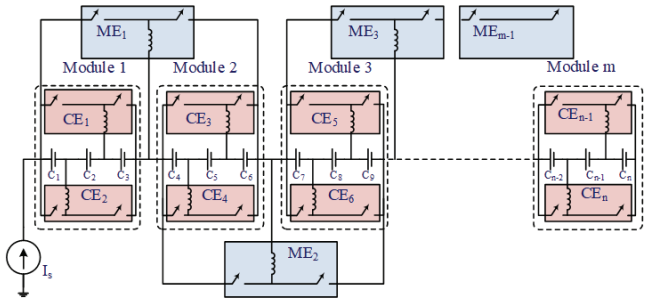

Fig. 1 Block diagram of proposed two-stage balancing circuit.

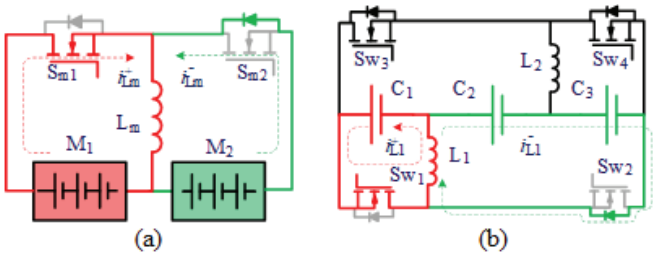

Fig. 2 (a) Module balancing circuit, (b) Cell balancing circuit.

II. Proposed Active Cell Balancing Topology

A. Circuit Structure

In this paper, a modularised two-stage active cell balancing circuit is proposed based on improved buck-boost converter circuit, and inductors are used to transfer energy from high charged cells/modules to low charged cells/modules.

Fig.1 shows the block diagram of modularized two-stage topology with 'm' number of modules and 'n' number of battery cells connected in series consisting of two stage balancing circuits. A battery pack with six cells is considered to demonstrate the operational principle of the proposed active cell balancing circuit with each module containing three number of cells. Fig. 2(a) shows the module balancing circuit which is worked based on the principle of buck-boost converter is comprised of five inductors (L_1, L_2, L_3, L_4 & L_m) and ten switches (Sw_1, Sw_2,...Sw_8 & Sm_1, Sm_2). Fig. 2(b) shows cell balancing circuit, which consist of three cells, two inductors (L_1& L_2) and four switches (Sw_1, Sw_2, Sw_3, Sw_4), to form single cell equalization unit.

B. Operational Principle

The equalizer in the proposed cell balancing circuit determines the operating modes and switching patterns based on the voltage difference of the modules/cells. The module/cell decides the source and target modules/cells with higher and lower voltages, respectively. Fig. 2(a) shows the proposed module balancing circuit where module M_1 is the source module and module M_2 is the target module, in which by controlling the switch S_{m1}, the charge can be transferred from the M_1 to M_2 by monitoring the voltages of two adjacent battery modules. The corresponding key waveforms are shown in Fig. 3(a). Similarly, charge can transfer from M_2 to M_1 by controlling switch S_{m2}. Unlike module balancing, by comparing the three cell voltages the balancing process will occur between the three cells and achieves the balance in cell balancing circuit. Fig. 2(b) shows the proposed cell balancing circuit where cell1 is the source cell and cell2 and cell3 are the target cells, in which by controlling the switch Sw_1, the charge is transferred from C_1 to C_2 & C_3. The corresponding key waveforms are shown in Fig. 3(b).

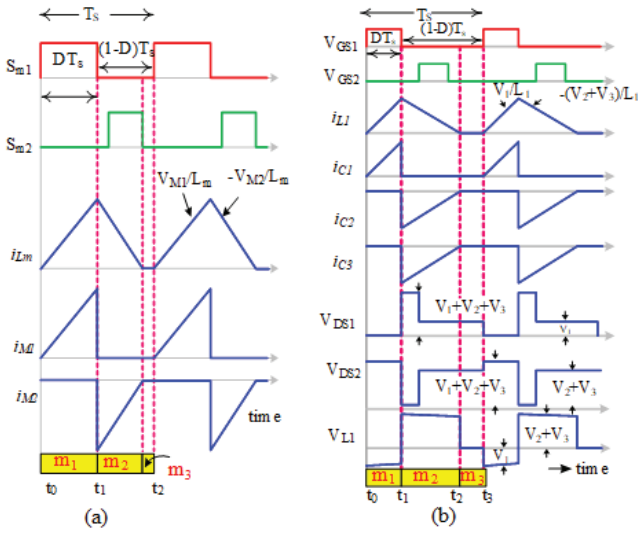

Fig. 3 Key waveforms for (a) Module balancing (b) Cell balancing

Similarly, by controlling the switches Sw_2, Sw_3 and Sw_4 the charge is transferred from C_2 & C_3 to C_1, C_1 & C_2 to C_3 and C_3 to C_1 & C_2 respectively.

C. Equalizing Currents formulation

1) Cell Equalizer Currents: To achieve cell balancing, the charge must be moved from the cell with maximum voltage to cell with minimum voltage by controlling equalizing currents with corresponding cell equalizers.

Let us consider the battery pack consisting of six cells that is composed of one module-based equalizer (ME_1), and four cell-based equalizers ($CE_{1,1}$, $CE_{1,2}$, $CE_{2,1}$, $CE_{2,2}$). Within the first module, the first cell-based equalizer ($CE_{1,1}$) can transmit charge among the cells in a bidirectional way with the equalizing currents defined as $I_{CEL_{1,1}} = i^{+}_{L1,1}$ and $I_{CER_{1,1}} = i^{-}_{L1,1}$ as shown in Fig. 4.

By comparing the cells voltages V_1, V_2, V_3 in the first battery module, the direction of equalizing current can be predetermined i.e. $I_{CEL_{1,1}}/I_{CER_{1,1}}$ is chosen as the controlled equalizing current, if the V_1/V_2&V_3 cell's voltage is greater than the V_2&V_3/V_1 cell's voltage. Then, a new non negative variable $I_{CE_{1,1}}$ can be used to replace $I_{CEL_{1,1}}$ and $I_{CER_{1,1}}$ such that

$$\begin{cases} I_{CEL_{1,1}} = \left(k_{1,1} + k'_{1,1}\alpha_{1,1}\right) I_{CE_{1,1}} \\ I_{CER_{1,1}} = \left(k_{1,1}\alpha_{1,1} + k'_{1,1}\right) I_{CE_{1,1}} \end{cases} \quad (1)$$

Case 1: If $(V_1 > V_2 \,\&\, V_3)$; With $k_{1,1} = 1, k'_{1,1} = 0$

$$i^{+}_{L1,1} = I_{CE_{1,1}} = I_{CEL_{1,1}} \quad (2)$$

$$i^{-}_{L1,1} = \alpha_{1,1} I_{CE_{1,1}} = I_{CER_{1,1}} \quad (3)$$

By substituting (2) in (3)

$$\alpha_{1,1} = \frac{i^{-}_{L1,1}}{i^{+}_{L1,1}} = \frac{I_{CER_{1,1}}}{I_{CEL_{1,1}}} \quad (4)$$

1) $i^{+}_{L1,1}$, $i^{-}_{L1,1}$ are the charging and discharging currents of inductor $L_{1,1}$. $I_{CEL_{1,1}}$, $I_{CER_{1,1}}$ represents the left and right-side currents of first cell-based equalizer in the first module.
2) $I_{CE_{1,1}}$ represents the controlled equalizing current of the first cell-based equalizer in the first battery module.
3) $\alpha_{1,1}\left(0 < \alpha_{1,1} \leq 1\right)$ is the charge transfer efficiency of the equalizer.

It should note that the direction of current out/in of the C_1/C_2 & C_3 cells is stated as the reference balancing current ($I_{E1,1}$) through first cell-based equalizer as shown in Fig. 4.

Similarly, the cell equalizer currents for case 2, case3 and case 4 are shown in Table I.

2) Module Equalizer Currents: Similarly, to achieve the module balancing, the module based equalizers will be used to transmit charge from the higher voltage battery module to lower voltage battery module, where the average voltage values of the cells will gives the voltage of the battery modules.

$$\begin{cases} I_{MEL_1} = \left(k_{M_1} + k'_{M_1}\alpha_{M_1}\right) I_{ME_1} \\ I_{MER_1} = \left(k_{M_1}\alpha_{M_1} + k'_{M_1}\right) I_{ME_1} \end{cases} \quad (5)$$

Case 1: If $(V_{M1} > V_{M2})$; With $k_{M1} = 1, k'_{M1} = 0$

$$i^{+}_{L_{M1}} = I_{ME_1} = I_{MEL_1} \quad (6)$$

$$i^{-}_{L_{M1}} = (\alpha_{M1}) I_{ME_1} = I_{MER_1} \quad (7)$$

By substituting (6) in (7)

$$\alpha_{M1} = \frac{i^{-}_{L_{M1}}}{i^{+}_{L_{M1}}} = \frac{I_{MER_1}}{I_{MEL_1}} \quad (8)$$

Case 2: If $(V_{M2} > V_{M1})$; With $k_{M1} = 0, k'_{M1} = -1$

$$\alpha_{M1} = \frac{i^{-}_{L_{M1}}}{i^{+}_{L_{M1}}} = \frac{I_{MEL_1}}{I_{MER_1}} \quad (9)$$

1) $i^{+}_{L_{M1}}$, $i^{-}_{L_{M1}}$ are the charging and discharging currents of inductor L_{M1}.
2) I_{ME_1} represents the controlled equalizing current of the first module equalizer (ME_1).
3) $\alpha_{ME1}(0 < \alpha_{M1} \leq 1)$ is the charge transfer efficiency of the first module equalizer.

3) Total Currents: As illustrated in Fig. 4, The equalizing current of a cells is comprised of currents flowing across its associated module-based and cell-based equalizers, and it can be determined by the following equations.

By applying KCL at 'a', 'b', 'c' and 'd' in Fig. 4, we get

$$\begin{cases} I_{E_{1,1}} = I_{C_{1,1}} = I_{CEL_{1,1}} + I_{MEL_1} \\ I_{E_{1,2\&3}} = I_{C_{1,2\&3}} = -I_{CER_{1,1}} + I_{MEL_1} \\ I_{E_{2,1}} = I_{C_{2,1}} = I_{CEL_{2,1}} - I_{MER_1} \\ I_{E_{2,2\&3}} = I_{C_{2,2\&3}} = -I_{CER_{2,1}} - I_{MER_1} \end{cases} \quad (10)$$

where $I_{E_{1,1}}$, $I_{E_{1,2\&3}}$, $I_{E_{2,1}}$ and $I_{E_{2,2\&3}}$ represents the equalizing current C_1, C_2 and C_3 in the first module and second module respectively, which is define as negative/positive when it charges/discharges the cell.

Then, by substituting (1) & (5) in (10), we get

$$\begin{cases} I_{E_{1,1}} = g_{1,1} I_{CE_{1,1}} + g_{M_1} I_{ME_1} \\ I_{E_{1,2\&3}} = -g'_{1,1} I_{CER_{1,1}} + g_{M_1} I_{ME_1} \\ I_{E_{2,1}} = g_{M_1} I_{CEL_{2,1}} - g'_{M_1} I_{MER_1} \\ I_{E_{2,2\&3}} = -g'_{M_1} I_{CER_{2,1}} - g'_{M_1} I_{MER_1} \end{cases} \quad (11)$$

With $g_{1,1} = k_{1,1} + k'_{1,1}\alpha_{1,1}$, $g'_{1,1} = k_{1,1}\alpha_{1,1} + k'_{1,1}$.
$g_{M_1} = k_{M_1} + k'_{M_1}\alpha_{M_1}$, $g'_{M_1} = k_{M_1}\alpha_{M_1} + k'_{M_1}$.

Hence, by comparing the present voltage values of nearby battery cells and modules, the gains $g_{1,1}$, $g'_{1,1}$, g_{M_1}, g'_{M_1} in (11) can be predetermined. They can be considered as known parameters while designing the control algorithm for cell equalization.

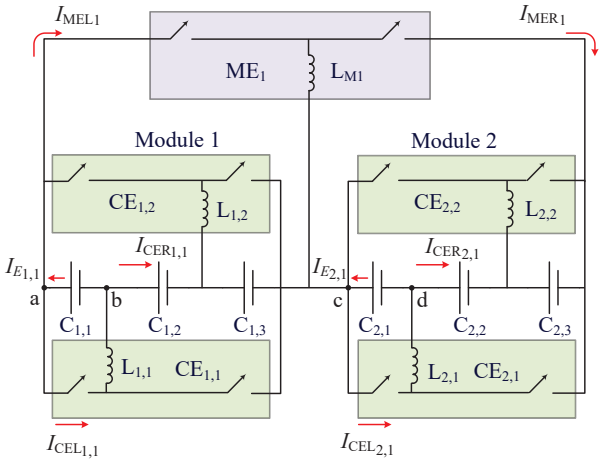

Fig. 4. Circuit for cell equalizing currents based on buck-boost converter.

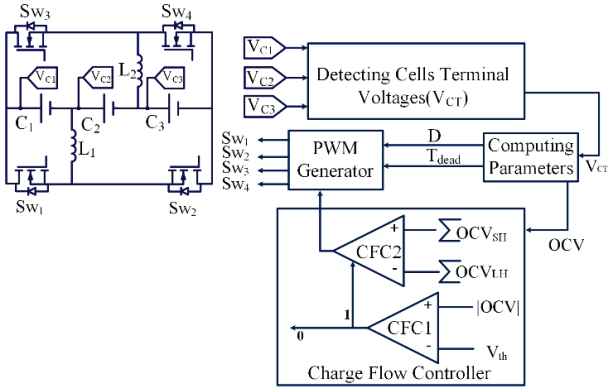

Fig. 5. Control strategy for the proposed cell balancing.

D. *Control strategy*

A control scheme is developed to analyse the equalization performance, as shown in Fig. 5. The controller detects the cell terminal voltages (V_{CT}). Based on the identified V_{CT}, the controlled parameter OCV is determined. According to OCV, the charge flow controller decides the charge flow direction and equalization action. CFC1 is used for issuing the true/false statements by comparing the OCV with the pre-set threshold voltage (V_{th}). When the OCV is greater than the threshold voltage value, the CFC1 gives the true signal, indicating that a voltage difference has been detected; Else it is not activated. Meantime, the CFC2 decides which cell has the highest voltage by comparing the sum of each cell's OCV. To decide the direction of power flow, the CFC2 combines with the true signal of CFC1. The gate signal is generated by the PWM generator using duty cycle D, and the power flow direction signal from CFC2.

III. Simulation and Experimental Validation

Simulated and experimental results for the proposed cell balancing circuit are presented in this section to validate the theoretical analysis and experimental viability.

A laboratory prototype for the proposed cell balancing circuit with three lithium-ion cells connected in series has been developed. To sense the cell voltage, each cell is equipped with the voltage sensor.

The FPGA controller calculates the pulse width modulation (PWM) duty cycles after receiving voltage data of the cell through an Analog-to-digital converter. The PWM gate pulse is applied to MOSFET switch via isolated gate driver.

Table I
CELL EQUALIZING CURRENTS OF CASE 2, CASE 3, CASE 4 FOR MODULE 1

$Case2(V_{C2}\&V_{C3} > V_{C1})$	$i^{+}_{L1,1} = I_{CE_{1,1}} = I_{CER_{1,1}}$	$i^{-}_{L1,1} = (\alpha_{1,1})I_{CE_{1,1}} = I_{CEL_{1,1}}$	$I_{E_{1,2\&3}} = I_{C_{1,2\&3}} = -I_{CER_{1,1}} + I_{MEL_1}$
$Case3(V_{C1}\&V_{C2} > V_{C3})$	$i^{+}_{L1,2} = I_{CE_{1,2}} = I_{CEL_{1,2}}$	$i^{-}_{L1,2} = (\alpha_{1,2})I_{CE_{1,2}} = I_{CER_{1,2}}$	$I_{E_{1,1\&2}} = I_{C_{1,1\&2}} = I_{CEL_{1,2}} + I_{MEL_1}$
$Case\ (V_{C3} > V_{C1}\&V_{C2})$	$i^{+}_{L1,2} = I_{CE_{1,2}} = I_{CER_{1,2}}$	$i^{-}_{L1,2} = (\alpha_{1,2})I_{CE_{1,2}} = I_{CEL_{1,2}}$	$I_{E_{1,3}} = I_{C_{1,3}} = -I_{CER_{1,2}} + I_{MEL_1}$

1) Simulation results

A. Case 1: ($V_{C1} > V_{C2}$ & V_{C3})

To evaluate the theoretical waveforms illustrated in Fig. 3(b), the simulation results are measured at $D = 0.4$. Fig. 6(a) represents the corresponding simulated waveforms about $I_{L1} \approx 1.6$A and $V_{DS1} \approx 4$V, $V_{DS2} \approx 8$V. Figs. 6(b) represents the simulated waveforms of current distribution among three battery cells, during the instant switch Sw_1 is turned on, the discharging current of cell C_1 increases with a constant slope. Further, the equalizing current from cell C_1 flows into C_2 and C_3 when Sw_1 is switched off and the current decreases with constant slope.

B. Case 2: (V_{C2} & $V_{C3} > V_{C1}$)

To evaluate the theoretical waveforms for case 2, the simulation results are measured at $D = 0.3$. Fig. 7(a) represents the corresponding simulated waveforms about $I_{L1} \approx 2.3$A and $V_{DS1} \approx 4$V, $V_{DS2} \approx 8$V. Fig. 7(b) represents the simulated waveforms of current distribution among three battery cells, during the instant switch Sw_2 is turned on, the discharging currents of cells C_2& C_3 increases with a constant slope. Further, the equalizing current from cell C_2 & C_3 flows into C_1 when Sw_2 is turned off and the current decreases with constant slope.

C. Case 3: (V_{C1} & $V_{C2} > V_{C3}$)

To evaluate the theoretical waveforms for case 3, the simulation results are measured at $D = 0.3$. Fig. 8(a) represents the corresponding simulated waveforms about $I_{L2} \approx 2.2$A and $V_{DS3} \approx 8$V, $V_{DS4} \approx 4$V. Fig. 8(b) represents the simulated waveforms of current distribution among three battery cells, during the instant switch Sw_3 is turned on, the discharging currents of cells C_1& C_2 increases with a constant slope. Further, the equalizing current from cell C_1 & C_2 flows into C_3 when Sw_3 is turned off and the current decreases with constant slope.

D. Case 4: ($V_{C3} > V_{C1}$ & V_{C2})

To evaluate the theoretical waveforms for case 4, the simulation results are measured at $D = 0.4$. Fig. 9(a) represents the corresponding simulated waveforms about $I_{L2} \approx 1.6$A and $V_{DS4} \approx 4$V, $V_{DS3} \approx 8$V. Figs. 9(b) represents the simulated waveforms of current distribution among three battery cells, during the instant switch Sw_4 is turned on, the discharging current of cell C_3 increases with a constant slope. Further, the equalizing current from cell C_3 flows into C_1 and C_2 when Sw_4 is switched off and the current decreases with constant slope.

E. Validation of the balancing effect

In order to know the balancing performance of the proposed circuit, the cell balancing process is conducted under different operating conditions are shown in Fig. 10.

The initial values for case 1 are 4.05V, 3.8V, 3.75V concerning C_1, C_2 and C_3. The equalization current flows from C_1 to C_3 is higher than C_2 because C_1 has the highest and C_3 has lowest voltages. The voltage gap between each pair of cells is maintained to be less than 0.02. After the equalization process starts with initial voltage difference between C_1 and C_3 is 0.3V. After entire equalization process of 700 seconds, the voltage difference is reduced from 0.3V to 18 mV as shown Fig. 10(a).

The initial values for case 2 are 3.8V, 4.05V, 4.1V concerning the C_1, C_2 and C_3. In this case the C_2 and C_3 are having the highest voltages and C_1 has the lowest voltage. After entire equalization process of 700 seconds, the voltage difference is reduced from 0.3V to 15 mV as shown Fig. 10(b).

The initial values for case 3 are 4.1V, 4.05V, 3.8V concerning C_1, C_2 and C_3. In this case the C_1 and C_2 are has highest voltages and C_3 has lowest voltage. After entire equalization process of 700 seconds, the voltage difference is reduced from 0.3V to 12 mV as shown Fig. 10(c).

In order to further verify the equalization performance, the initial values for case 4 are 3.75V, 3.8V, 4.1V concerning the C_1, C_2 and C_3. The equalization current flows from C_3 to C_1 is higher than C_2 because C_3 has the highest and C_1 has lowest voltages. After entire equalization process of 700 seconds, the voltage difference is reduced from 0.35V to 20 mV as shown Fig. 10(d).

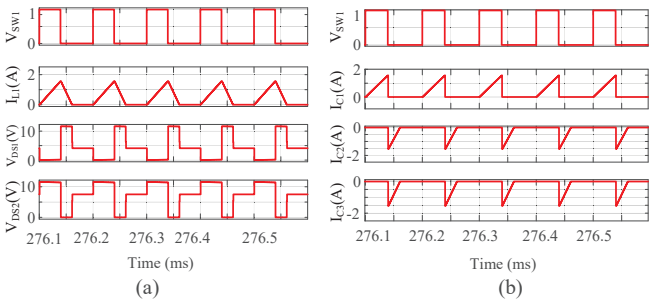

Fig. 6 Simulation waveforms of CASE 1 ($V_{C1} > V_{C2}$ & V_{C3}) (a) V_{GSw1}, I_{L1}(A), V_{DSw1}, V_{DSw2} (b) V_{GSw1}, I_{C1}(A), I_{C2}(A), I_{C3}(A).

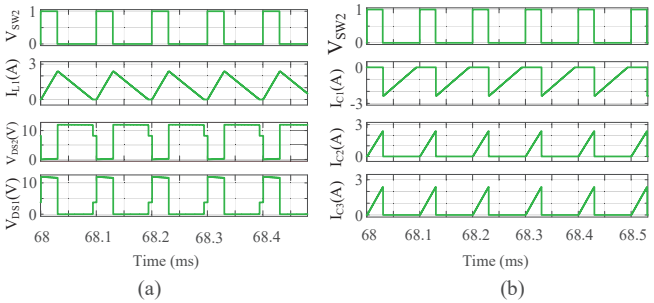

Fig. 7 Simulation waveforms of CASE 2 (V_{C2} & $V_{C3} > V_{C1}$) (a) V_{GSw2}, I_{L1}(A), V_{DSw2}, V_{DS3} (b) V_{GSw2}, I_{C1}(A), I_{C2}(A), I_{C3}(A).

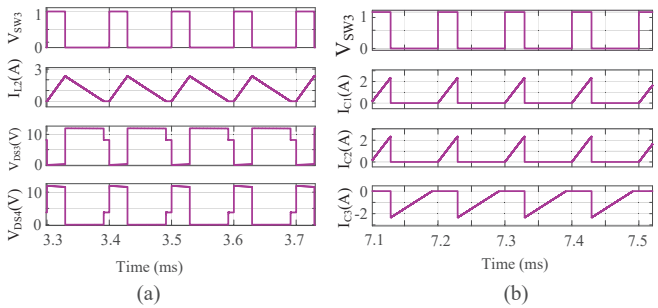

Fig. 8 Simulation waveforms of CASE 3 (V_{C1} & $V_{C2} > V_{C3}$) (a) V_{GSw3}, I_{L2}(A), V_{DSw3}, V_{DSw4} (b) V_{GS3}, I_{C1}(A), I_{C2}(A), I_{C3}(A).

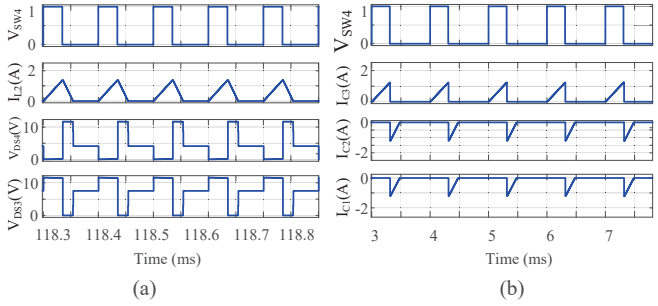

Fig. 9 Simulation waveforms of CASE 4 ($V_{C3} > V_{C1}$ & V_{C2}) (a) V_{GSw4}, I_{L2}(A), V_{DSw4}, V_{DSw3} (b) V_{GSw4}, I_{C1}(A), I_{C2}(A), I_{Cw3}(A).

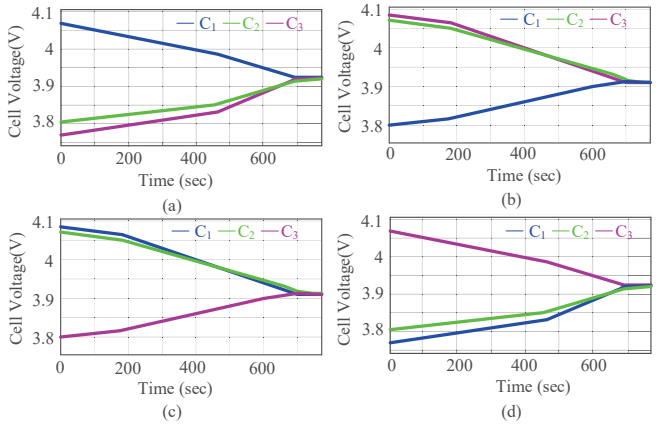

Fig. 10 Simulation waveforms of cell voltages during the cell equalization process of four cases (a) Case 1($V_{C1} > V_{C2}$ & V_{C3}) (b) Case 2 (V_{C2} & $V_{C3} > V_{C1}$), (c) Case 3 (V_{C1} & $V_{C2} > V_{C3}$), (d) Case 4 ($V_{C3} > V_{C1}$ & V_{C2})

2) Experimental results

To verify the feasibility of the control strategy, an experiment is conducted for case 1 under the static condition with different initial Li-ion cell voltages.

Fig. 11(a) shows experimental waveforms of inductor current $I_{L1} \approx 1.6$ A,voltage stress across switch Sw_1 and Sw_2 i.e. $V_{DSw1} \approx 3.995$V and $V_{DS2} \approx 7.98$V respectively. Fig. 11(b) illustrate the cell currents during equalization. It is notable that the experimental waveforms are almost matchup with simulated waveforms shown in 6 (a) and (b).

Fig. 11(c) illustrates the cell equalization process for case1 with the initial values are 3.9V, 3.8V, 3.75V concerning C_1, C_2 and C_3. After the equalization process starts with initial voltage difference between C_1 and C_3 is 150 mV. After entire equalization process of 700 seconds, the voltage difference is reduced from 150 mV to 16 mV.

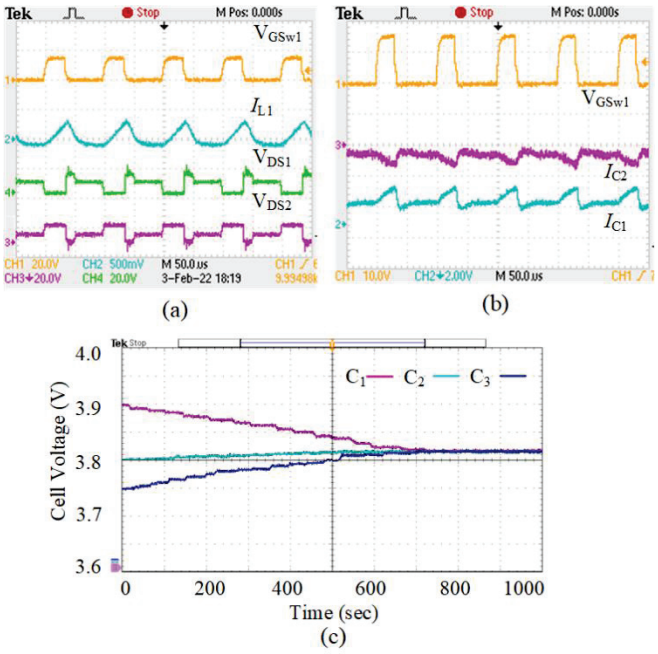

Fig. 11 Experimental waveforms of CASE 1 ($V_{C1} > V_{C2}$ & V_{C3}) (a) V_{GS1}, I_{L1}(A), V_{DS1}, V_{DS2} (b) V_{GS1}, I_{C1}(A), I_{C2}(A) (c) Cell voltages during equalization process.

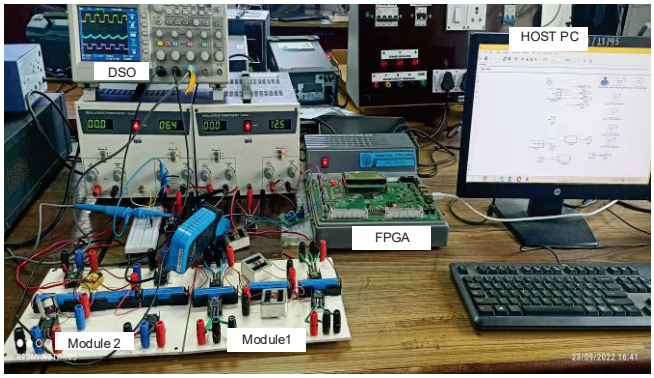

Fig. 12 Experimental setup.

IV. Conclusion

A modularized two-stage active cell balancing circuit based on an improved buck-boost converter is proposed in this paper. By transferring the high balancing current from the string to the weakest cell in a module directly, the proposed cell balancing circuit significantly reduces the balancing time with fewer number of components. Due to modulization technique used, voltage stress on the switches is reduced, which can greatly improve the system performance. A laboratory prototype of the proposed active cell balancing topology is designed and implemented. An extensive test has been conducted for the laboratory prototype to validate the proposed circuit and it has been validated with different initial cell voltage conditions, and the results are found satisfactory. The cell equalization time is found to be 700s with the proposed circuit, which is significantly less compared to conventional circuits. Therefore, the proposed active cell balancing circuit is a suitable for equalizing Li-ion cells in the battery packs.

REFERENCES

[1] N. Ghaeminezhad, Q. Ouyang, X. Hu, G. Xu and Z. Wang, "Active Cell Equalization Topologies Analysis for Battery Packs: A Systematic Review, "*IEEE Trans. Power Electron.*, vol. 36, no. 8, pp. 9119-9135, Aug.2021.

[2] J. G. Lozano, E. R. Cadaval, M. I. M. Montero, and M. A. G. Martinez, "A novel active battery equalization control with on-line unhealthy cell detection and cell change decision," J. Power Sources, vol. 299, pp. 356– 370, Dec. 2015.

[3] J. W. Kimball, B. T. Kuhn, and P. T. Krein, "Increased performance of battery packs by active equalization," in *2007 IEEE Vehicle Power and Propulsion Conference*, Sept 2007, pp. 323–327.

[4] H. S. Park, C. E. Kim, C. H. Kim, G. W. Moon, and J. H. Lee, "A modularized charge equalizer for an HEV lithium-ion battery string, *IEEE Transactions on Industrial Electronics*, vol. 56, no. 5, pp. 1464–1476, May 2009.

[5] P. A. Cassani and S. S. Williamson, "Feasibility analysis of a novel cell equalizer topology for plug-in hybrid electric vehicle energy-storage systems," *IEEE Transactions on Vehicular Technology*, vol. 58, no. 8, pp. 3938–3946, Oct 2009.

[6] M. Lee, S.-W. Lee, Y.G. Choi, and B. Kang, "Active balancing of Li-ion battery cells using transformer as energy carrier," *IEEE Trans. Ind. Electron.*, vol. 64, no. 2, pp. 1251–1257, Feb. 2017.

[7] F. Peng, H. Wang and L. Yu, "Analysis and Design Considerations of Efficiency Enhanced Hierarchical Battery Equalizer Based on Bipolar CCM Buck–Boost Units, "*IEEE Trans. Ind. Appl*, vol. 55, no. 4, pp. 4053-4063, July-Aug. 2019 .

[8] F. Baronti, G. Fantechi, R. Roncella and R. Saletti, "High-Efficiency Digitally Controlled Charge Equalizer for Series-Connected Cells Based on Switching Converter and Super-Capacitor, "*IEEE Trans. Ind. Inform.*, vol. 9, no. 2, pp. 1139-1147, May 2013.

[9] K. -M. Lee, Y. -C. Chung, C. -H. Sung and B. Kang, "Active Cell Balancing of Li-Ion Batteries Using LC Series Resonant Circuit, "*IEEE Trans. Ind. Electron*, vol. 62, no. 9, pp. 5491-5501, Sept. 2015.

[10] T. H. Phung, A. Collet and J. Crebier, "An Optimized Topology for Next-to-Next Balancing of Series-Connected Lithium-ion Cells," *IEEE Trans. Power Electron.*, vol. 29, no. 9, pp. 4603-4613, Sept. 2014.

[11] S. Yarlagadda, T. T. Hartley and I. Husain, "A Battery Management System Using an Active Charge Equalization Technique Based on a DC/DC Converter Topology, "*IEEE Trans. Ind. Appl.*, vol. 49, no. 6, pp. 2720-2729, Nov.-Dec. 2013.

[12] F. Peng, H. Wang and L. Yu, "Analysis and Design Considerations of Efficiency Enhanced Hierarchical Battery Equalizer Based on Bipolar CCM Buck–Boost Units, "*IEEE Trans. Ind. Appl*, vol. 55, no. 4, pp. 4053-4063, July-Aug. 2019.